

Green Synthesized Iron Oxide Nanoparticles Effect on Fermentative Hydrogen Production by *Clostridium acetobutylicum*

Sundaresan Mohanraj · Shanmugam Kodhaiyolii ·
Mookan Rengasamy · Velan Pugalenthi

Received: 2 December 2013 / Accepted: 28 February 2014 /
Published online: 20 March 2014
© Springer Science+Business Media New York 2014

Abstract A green synthesis of iron oxide nanoparticles (FeNPs) was developed using *Murraya koenigii* leaf extract as reducing and stabilizing agent. UV–vis spectra show that the absorption band centred at a wavelength of 277 nm which corresponds to the surface plasmon resonances of synthesized FeNPs. Fourier transform infrared spectroscopy spectrum exhibits that the characteristic band at 580 cm^{-1} is assigned to Fe–O of $\gamma\text{-Fe}_2\text{O}_3$. Transmission electron microscopy image confirms that the spherical with irregular shaped aggregates and average size of nanoparticles was found to be ~ 59 nm. The effect of synthesized FeNPs on fermentative hydrogen production was evaluated from glucose by *Clostridium acetobutylicum* NCIM 2337. The hydrogen yield in control experiment was obtained as 1.74 ± 0.08 mol H_2 /mol glucose whereas the highest hydrogen yield in FeNPs supplemented experiment was achieved as 2.33 ± 0.09 mol H_2 /mol glucose at 175 mg/L of FeNPs. In addition, the hydrogen content and hydrogen production rate were also increased from 34 ± 0.8 to 52 ± 0.8 % and 23 to 25.3 mL/h, respectively. The effect of FeNPs was compared with supplementation of FeSO_4 on fermentative process. The supplementation of FeNPs enhanced the hydrogen production in comparison with control and FeSO_4 . The supplementation of FeNPs led to the change of the metabolic pathway towards high hydrogen production due to the enhancement of ferredoxin activity. The fermentation type was shifted from butyrate to acetate/butyrate fermentation type at the addition of FeNPs.

Keywords Green synthesis · Iron oxide nanoparticles · *Murraya koenigii* · Hydrogen production · *Clostridium acetobutylicum* NCIM 2337

S. Mohanraj · S. Kodhaiyolii · V. Pugalenthi (✉)
Department of Biotechnology, Bharathidasan Institute of Technology, Anna University, Tiruchirappalli 620
024 Tamil Nadu, India
e-mail: pugalv@gmail.com

M. Rengasamy
Department of Petrochemical Technology, Bharathidasan Institute of Technology, Anna University,
Tiruchirappalli 620 024 Tamil Nadu, India

Introduction

Metal and metal oxide nanoparticles have been attracting significant interest because of their various applications. Metal oxide nanoparticles have unique physical and chemical properties due to their small size and high surface area. Among the metal oxide nanoparticles, iron oxide nanoparticles are having different forms such as magnetite (Fe_3O_4), hematite ($\alpha\text{-Fe}_2\text{O}_3$) and maghemite ($\gamma\text{-Fe}_2\text{O}_3$) [1]. Iron oxide nanoparticles have recently gained enormous interest in various processes such as wastewater treatment [2] and biocatalysis [3] because of their large surface area, high surface reactivity and high sorption capacity. Several methodologies have been established to synthesize iron oxide nanoparticles including physical and chemical methods. However, environmental contamination is a major concern in the chemical synthesis of metal nanoparticles. To avoid the environmental contaminations, the rapid development of cost-effective, non-toxic and eco-friendly process is needed for synthesizing iron oxide nanoparticles. Biosynthesis of metal nanoparticles using microorganisms and plants are considered as simple, green and cost-effective methods [4].

Plant extract-mediated synthesis of nanomaterials is one of the more stable and suitable alternatives in comparison with those produced by physical, chemical and microbial methods. The synthesis of metal oxide nanoparticles using plant extracts has been found to be faster than the microbial synthesis. The green method has been growing significance due to its simplicity and eco-friendliness. In addition, this process would impart steric stabilization against aggregation and also help to overcome the environmental contaminations [5]. Recently, green synthesis of iron nanoparticles of various shape and size has been developed using green tea [5–7], soya bean sprouts [8] and sorghum bran extracts [9]. In continuation of the efforts, the aromatic leaves of *Murraya koenigii* has been used for the reduction and stabilization of silver nanoparticles [10]. Philip et al [10] and Christensen et al. [11] also reported that the high concentration of water-soluble ingredients such as carbazole, alkaloids, flavonoids and polyphenols in *M. koenigii* leaf extract has been identified as responsible for rapid reduction and stabilization of silver nanoparticles. However, the potential of *M. koenigii* for the synthesis of other metal and metal oxide nanoparticles has yet to be fully explored. To the best of our knowledge, there is no report on the development of rapid method for green synthesis of iron oxide nanoparticles using aqueous *M. koenigii* leaf extract.

Hydrogen as a green energy source is considered as an alternative energy to substitute fossil fuels in the future due to its ideal and clean characteristics. Among the various hydrogen production technologies, fermentative process for hydrogen production has more potential because it is a promising way to produce more energy from organic substrate [12]. Nevertheless, the supplementation of suitable micronutrients is required to improve the fermentative process for efficient hydrogen production. Iron, magnesium, zinc, sodium [13] and nickel [14] are all important trace metals for fermentative hydrogen production. Among the trace metals, iron plays important roles in electron transport, enhancing bacterial growth and high rate hydrogen production by promoting hydrogenase activity [14]. According to the previous report, supplementation of iron could oxidize the reduced ferredoxin to produce more hydrogen [13]. Especially, iron is a component of ferredoxin which acts as an electron carrier in hydrogenase to produce molecular hydrogen. Recently, few studies have been investigated on fermentative hydrogen production from glucose by the supplementation of Fe^{2+} using mixed culture [15, 16], but there is no report to evaluate the effects of Fe^{2+} and iron oxide nanoparticles on fermentative hydrogen production from glucose by *Clostridium acetobutylicum*. In addition, the efficient conversions of substrate, high yields of hydrogen and high rate process for fermentative hydrogen production have not been achieved. Hence, the supplementation of synthesized iron oxide nanoparticles was considered in the present study for enhancement of fermentative hydrogen production.

The objective of this study was to develop a facile and rapid green synthesis of iron oxide nanoparticles using a non-toxic, renewable plant *M. koenigii* leaf extract as both the reducing and stabilizing agent. The effects of synthesised iron oxide nanoparticles and FeSO_4 on fermentative hydrogen production from glucose using *C. acetobutylicum* NCIM 2337 were investigated to find out the enhancement efficiency. The obtained hydrogen production data were used to fit the Gompertz equation for kinetic analysis of fermentative process.

Materials and Methods

Materials

The leaves of *M. koenigii* (curry leaves) were obtained from the local market of Tiruchirappalli, Tamil Nadu, India. The fermentative medium ingredients including FeSO_4 , KH_2PO_4 , Na_2HPO_4 , NH_4Cl , MgCl_2 , yeast extract, meat extract, peptone and glucose were purchased from Himedia, India. *C. acetobutylicum* NCIM 2337 was obtained from National Chemical Laboratory, Pune, India. All the experiments were performed in triplicates. Double distilled water was used for all the experiments.

Preparation of *M. koenigii* Leaf Extract

M. koenigii leaves were washed with deionized water and dried at room temperature for 24 h. Four grams of finely powdered leaf was mixed with 100 mL distilled water in an Erlenmeyer flask. The extract from *M. koenigii* leaves was done on boiling water bath at 100 °C for 5 min. The leaf extract was filtered through Whatman no. 1 filter paper and the filtrate was stored at 4 °C for further experiments.

Green Synthesis of Iron Oxide Nanoparticles

To prepare the iron oxide nanoparticles, 3 mL of *M. koenigii* broth was added to 7 mL aqueous solution of 1 mM FeSO_4 and stirred for 5 min. The colour change was observed from transparent yellow to black after 5 min, indicating the formation of iron nanoparticles. One, 2 and 3 mL of *M. koenigii* leaf extract was separately added to 9, 8 and 7 mL of 1 mM FeSO_4 concentration, respectively, in order to investigate the effect of *M. koenigii* extract on the formation of iron oxide nanoparticles. Seven millilitres of 0.25, 0.5 and 1 mM FeSO_4 concentration was separately taken and mixed with 3 mL of *M. koenigii* leaf extract to find out the optimum concentration. All the experiments were performed on a magnetic stirrer at room temperature. The resulting iron colloids were centrifuged (15,000 rpm, 20 °C) for 20 min, washed several times with distilled water and dried at a hot air oven.

Effect of Iron Oxide Nanoparticles on Fermentative Hydrogen Production

C. acetobutylicum NCIM 2337 was cultivated in Reinforced Clostridial Broth (Himedia laboratories) under anaerobic condition for 24 h at 37 °C. Fermentative hydrogen production was conducted in 250 mL bottle with a working volume of 200 mL. Fermentative hydrogen-producing medium contained the following compositions (g/L): 1.5 KH_2PO_4 , 3.2 Na_2HPO_4 , 0.5 NH_4Cl , 0.8 MgCl_2 , 1.0 yeast extract, 0.5 meat extract, 0.5 peptone and 7.5 glucose. The concentrations of iron oxide nanoparticles and FeSO_4 were taken in the range from 0 to 250 mg/L for evaluating the enhancement effect of hydrogen production. The fermentation

medium was adjusted to pH 6.0 and the duration of fermentation was about 24 h. The headspace air was displaced by nitrogen gas to generate anaerobic condition in the reactor. The produced hydrogen was collected in a gas collector by water displacement method. The volume of the hydrogen and glucose utilization was measured at different time intervals.

Characterization of Iron Oxide Nanoparticles

The bioreduction of Fe^{2+} ions was monitored as a function of reaction time by using Varian, Cary 100 UV–vis spectrophotometer in the range of 200–800 nm. Fourier transform infrared spectroscopy (FTIR) analysis of iron oxide nanoparticles was carried out by PerkinElmer, Spectrum RX1. Morphology and size distribution of iron oxide nanoparticles were performed using scanning electron microscopy (SEM—JEOL JSM 5610) and transmission electron microscopy (TEM—Tecnai 10; Philips). The size distribution of the iron oxide nanoparticles obtained from TEM micrographs was analysed using a speciality image processing software ImageJ 1.45. The particle size distribution of iron oxide nanoparticles size was measured using a Zetasizer Nano ZS 90 (Malvern Instruments).

Analytical Methods

The composition of biogas including H_2 , CO_2 and CH_4 was analysed by Shimadzu gas chromatograph (GC-2014) (Shimadzu Co. Singapore) equipped with a thermal conductivity detector and a stainless steel column packed with Porapak Q (80/100 mesh). The operational temperatures at the injection port, column oven and detector were 40, 40 and 80 °C, respectively. Nitrogen was used as carrier gas at a flow rate of 20 mL/min. The concentration of the volatile fatty acids (VFAs) was measured by Shimadzu gas chromatograph (GC-2014) (Shimadzu Co. Singapore) equipped with a flame ionization detector (FID) and stabilwax–DA capillary column. The injector, column oven and detector were operated at 180, 200 and 220 °C, respectively. Nitrogen was used as carrier gas with a flow rate of 5 mL/min. The concentration of glucose was determined using phenol–sulphuric acid method [17].

Kinetic Modelling Analysis

The modified Gompertz equation was used in this study to illustrate the modelling of fermentative hydrogen production in batch experiments.

$$H = P \cdot \exp\{-\exp[\text{Rm} \times e/P(\lambda - t) + 1]\}$$

where H denotes the cumulative volume of hydrogen production (mL), P is hydrogen production potential (mL), Rm represents the maximum hydrogen production rate (mL/h), e is 2.71828, λ represents the lag-phase time (h), and t denotes the incubation time (h). The kinetic parameters (P , Rm and λ) were estimated by Origin 7.5 [18].

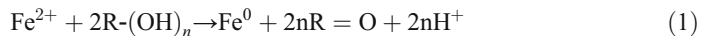
Results and Discussion

UV–Visible Spectrums of Iron Oxide Nanoparticles

The formation of iron oxide nanoparticles was observed with the colour change and UV–visible spectral analysis. The different concentrations of *M. koenigii* leaf extract (1, 2 and

3 mL) on the reduction of Fe^{2+} ions was monitored by using UV–vis spectroscopy. The light black colour of the iron colloids was formed by the addition of 1 and 2 mL of leaf extract concentration, whereas the dark black colour was rapidly formed for completion of the reaction within 5 min by the addition of 3 mL leaf extract. The optimum concentration of leaf extract on different FeSO_4 concentration (0.25, 0.5 and 1.0 mM) was investigated (data not shown). The experimental results showed that there was no colour formation at 0.25 mM and the light black colour was observed at 0.5 mM, due to the slow reduction of ferrous ions. The colour of the reaction mixture was changed from transparent yellow to black colour within 5 min, after addition of 3 mL extract into 1 mM FeSO_4 solution. The formation of black colour solution indicated the rapid reduction of ferrous ions.

From the UV–visible spectra (Fig. 1a), it was observed that the two absorption peaks were detected at 284 and 315 nm as the concentration of *M. koenigii* leaf extract was increased. The appearance of two peaks indicated the formation of anisotropic iron oxide nanoparticles. According to Mie's theory, spherical or quasi-spherical nanocrystals exhibit a single surface plasmon resonance (SPR) band, whereas anisotropic particles show two or three bands, depending on their shape [19]. Furthermore, the disappearance of peak at 315 nm and slight blue shift in the peak from 284 to 277 nm was observed after 3 h. This result indicates the formation of $\text{Fe}(0)$ nanoparticles because no absorption peak was observed in FeSO_4 solution as illustrated previously by Guo et al. [20]. As seen in traces (4–7 h) in Fig. 1a, the decrease in intensity of peak at 277 nm may be due to the oxidation of zero valent iron to iron oxide nanoparticles. Similar observation was reported earlier [20]. Therefore, the proposed possible mechanism for synthesizing iron oxide nanoparticles is given below (Eqs. 1 and 2);



FTIR Studies

FTIR analysis was used to identify the possible functional groups and capping agent present in *M. koenigii* leaf extract for the reduction of ferrous ions. Figure 1b shows the FTIR spectra of both synthesized iron oxide nanoparticles and *M. koenigii* leaf extract. The FTIR spectrum of

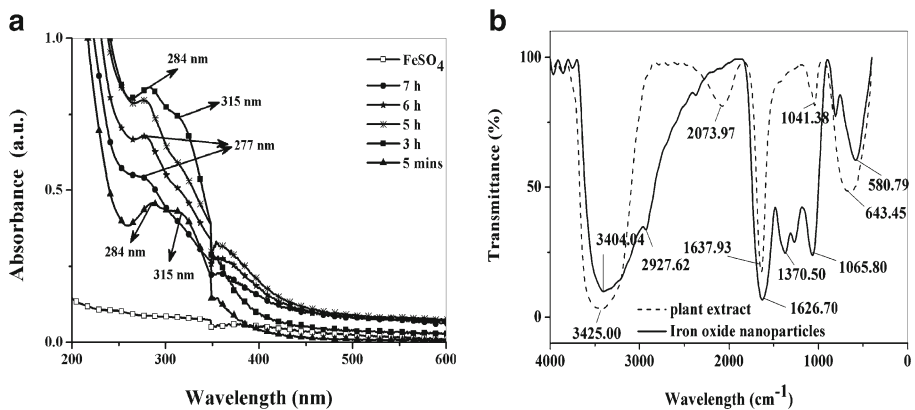


Fig. 1 a UV–visible absorption spectra of reaction mixtures at different time intervals. b FTIR spectra of *M. koenigii* leaf extracts (broken line) and synthesized iron oxide nanoparticles (solid line)

the leaf extract (broken line) showed bands at 3,425, 2,073, 1,637, 1,041 and 643 cm^{-1} . The intense broad absorbance at 3,425 cm^{-1} is attributed to the O–H stretching vibration of hydroxyl functional group in alcohols. The weak absorbance at 2,073 cm^{-1} may be assigned to the primary amines due to the presence of amino acids. The intense band at 1,637 cm^{-1} is assigned to the amide I band of the proteins released by the *M. koenigii* leaf extract. Similar trend was observed by Narayanan and Sakhthivel [21]. The band at 1,041 cm^{-1} is attributed to the C–N stretching vibration of aliphatic amines. The band at 643 cm^{-1} may be attributed to the C–H bending vibrations. The FTIR spectrum of synthesized iron oxide nanoparticles (solid line) showed bands at 3,404, 2,927, 1,626, 1,370, 1,065 and 580 cm^{-1} . The bands at 3,404 and 1,626 cm^{-1} are assigned to the hydroxyl group and proteins, respectively. The absorption peak at 2,927 cm^{-1} is designated to C–H stretching vibration modes in the hydrocarbon chains. The band at 1,370 cm^{-1} may be assigned to C–N stretching or the O–H bending. The band at 1,065 cm^{-1} is attributed to the C–N stretching vibration of aliphatic amines. The presence of iron oxide nanoparticles was identified by the strong absorption band at 580 cm^{-1} , which is assigned to the Fe–O bond of γ - Fe_2O_3 . Similar results were reported by earlier literature [22, 23]. The absorption band at 3,404, 1,626 and 1,065 cm^{-1} indicated that the synthesized iron oxide nanoparticles may be surrounded by polyphenols, proteins and amines. These findings indicate that the biomolecules present in the *M. koenigii* leaf extract may be accountable for the reduction of Fe^{2+} ions and stabilization of iron nanoparticles in an aqueous medium. Similarly, Philip et al. [10] reported that the biomolecules including flavonoids, alkaloids and polyphenols compounds present in the *M. koenigii* leaf extract were believed to be responsible for the reduction and efficient stabilization of silver and gold nanoparticles.

SEM, TEM and DLS Analysis

The surface morphology of the synthesized iron oxide nanoparticles was studied using SEM at a magnification of $\times 5,000$ (Fig. 2a). SEM images reveal that the synthesized iron oxide nanoparticles were aggregated into irregular with no well-defined structure (Fig. 2a). The morphology of the nanoparticles was mostly appeared to be a porous, spongelike form. The formation of various particles sizes may be due to the agglomeration of nanoparticles during the sample preparation for SEM analysis, as reported earlier [24]. From TEM images (Fig. 2b), it is evident that the morphology of iron oxide nanoparticles was spherical along with some irregular shape, which is in agreement with the shape of SPR band in the UV–vis spectra (Fig. 1a). The result of the TEM analysis confirms the amorphous nature of the iron oxide nanoparticles. The mean size of the amorphous iron oxide nanoparticles was determined as ~ 59 nm by ImageJ software tool. The particle size distribution of the iron oxide nanoparticles was analysed by dynamic light scattering analysis and the average size of iron oxide nanoparticles was found to be ~ 61 nm (Fig. 2c).

Effect of Iron Oxide Nanoparticles on Biohydrogen Production

The effects of FeSO_4 and iron oxide nanoparticles on fermentative hydrogen production using *C. acetobutylicum* NCIM 2337 are shown in Fig. 3. The hydrogen production of 254 ± 12 mL was observed in control experiment (without supplementation). However, the hydrogen production was considerably increased at 50 mg/L of FeSO_4 and it was decreased with increase of FeSO_4 concentration in the range from 100 to 250 mg/L. The maximum hydrogen production of 273 ± 11 mL was obtained at 50 mg/L of FeSO_4 supplementation. The addition

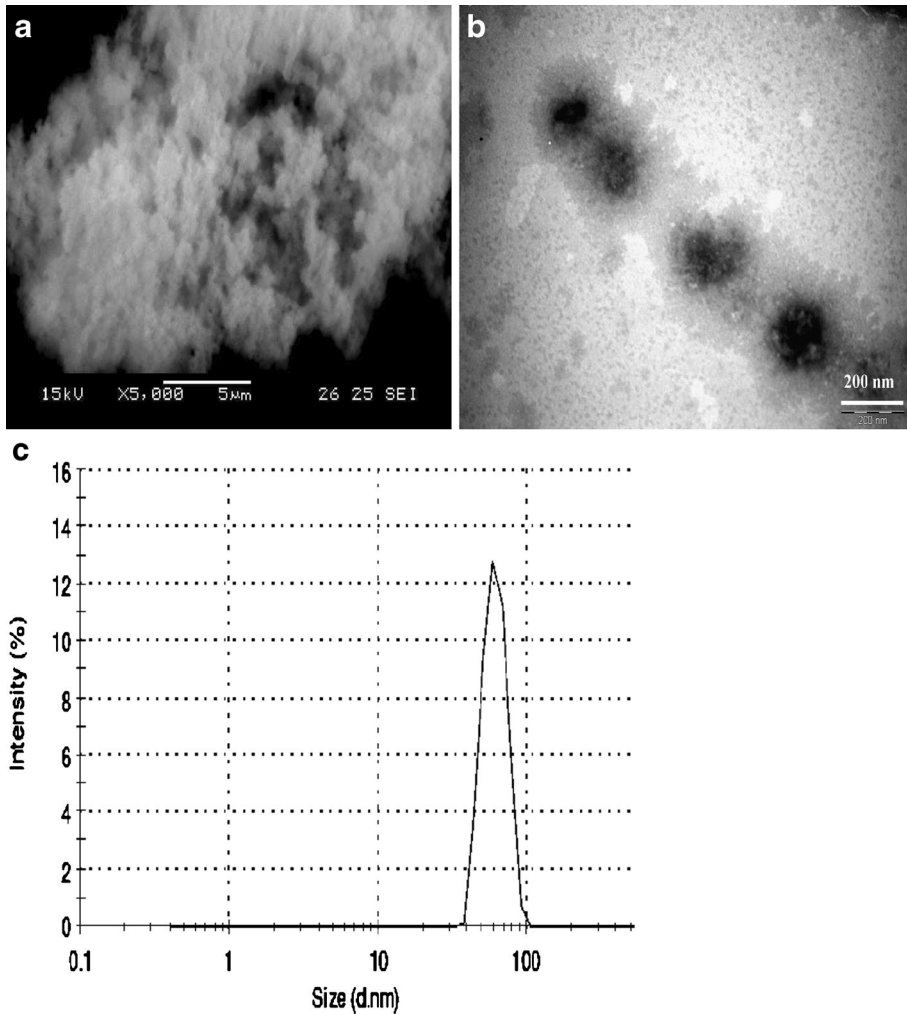


Fig. 2 **a** SEM image of iron oxide nanoparticles at $\times 5,000$ magnification. **b** TEM image of iron oxide nanoparticles at bar scale 200 nm. **c** Size distribution of iron oxide nanoparticles by dynamic light scattering

of 50 mg/L of FeSO_4 improved the hydrogen production, whereas the addition of low concentrations (below 50 mg/L; data not shown) and high concentrations (above 50 mg/L) suppressed the activity of *C. acetobutylicum*, resulting low hydrogen production. A similar result was also reported by Karadag and Puhakka [16]. They also found that the optimum concentration of 50 mg/L supplementation of Fe^{2+} was able to produce the maximum hydrogen production from glucose using mixed cultures. Despite that, the maximum hydrogen production of 314 ± 4 mL was achieved at 175 mg/L of FeNPs supplementation and it was decreased with increase of FeNPs concentration at above 175 mg/L. This result concludes that the addition of much lower (below 50 mg/L) and much higher concentrations (above 175 mg/L) of FeNPs was not suitable to increase the activity of *C. acetobutylicum*. The FeNPs-supplemented experiments exhibited that the hydrogen production was higher than the FeSO_4 supplementation. The results of the study suggest that the ferredoxin activity may be enhanced

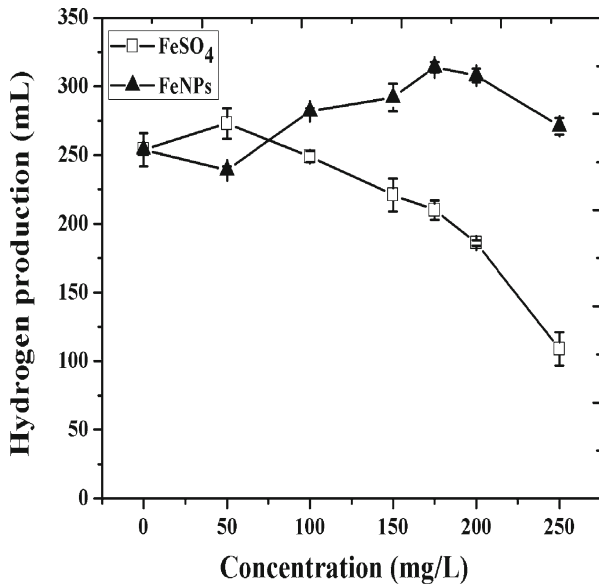


Fig. 3 Hydrogen production versus different concentration of FeSO₄ and FeNPs

by the supplementation of FeNPs during the fermentation process. According to the literature, the supplementation of Fe²⁺ improved the hydrogenase activity, which led to enhance the fermentative hydrogen production [15].

Figure 4a shows the experimental data of hydrogen yield and glucose utilization efficiency by *C. acetobutylicum*. The experimental data indicate that the hydrogen yield of 2.06 ± 0.08 mol H₂/mol glucose was found at 50 mg/L of FeSO₄ supplementation. Further, it was decreased with increase of FeSO₄ concentration at above 50 mg/L. As seen in the Fig. 3, the glucose utilization efficiency was drastically decreased at above 100 mg/L of FeSO₄ supplementations which led to decrease the hydrogen production. On the contrary, the glucose utilization efficiency was gradually decreased with increase of FeNPs concentrations from 0

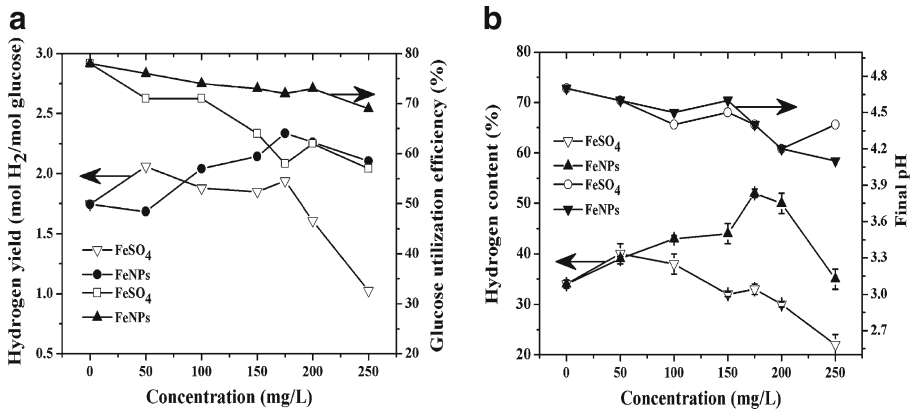


Fig. 4 a Effects of FeSO₄ and FeNPs on hydrogen yield and glucose utilization efficiency. **b** Effects of FeSO₄ and FeNPs on hydrogen content and final pH

to 250 mg/L. Meanwhile, the hydrogen yield was increased from 50 to 175 mg/L. These findings suggest that the bioactivity of *C. acetobutylicum* was enhanced up to 175 mg/L of FeNPs supplementation, when compared to FeSO₄. The FeNPs-supplemented experiments showed that the maximum hydrogen yield of 2.33 ± 0.09 mol H₂/mol glucose was observed at 175 mg/L of FeNPs. Moreover, the much higher concentrations of FeNPs at above 175 mg/L were not favourable for the *C. acetobutylicum* to increase the hydrogen yield during fermentative hydrogen production. The obtained yield was comparatively higher than the control experiment (1.74 ± 0.08 mol H₂/mol glucose). Recent report shows that the maximum hydrogen yield of 1.08 ± 0.06 mol H₂/mol glucose was obtained at the addition of 10^{-6} mol L⁻¹ concentration of encapsulated iron oxide nanoparticles with porous silica matrix (Fe/SiO₂) [25]. In comparison, the FeNPs supplementation in our experiments without any encapsulation method produced the maximum hydrogen yield of 2.33 ± 0.09 mol H₂/mol glucose. The similar trend was observed in hydrogen content which is presented in Fig. 4b. This figure shows the comparative study of FeSO₄ and FeNPs effects on hydrogen content and final pH during fermentative hydrogen production process. The final pH was decreased with increase of FeNPs and FeSO₄ concentrations from 0 to 200 mg/L. The results showed that the final pH values in all batch tests were lower than the initial pH 6.0 and it was gradually decreased up to 150 mg/L of FeNPs and FeSO₄. It was also noted that the final pH values were identified at below 4.5, when the supplements of FeNPs and FeSO₄ were varied from 150 to 250 mg/L. This result reveals that the low pH value at below 4.5 was not favourable for fermentative hydrogen production. Therefore, the hydrogen yield and glucose utilization efficiency in batch tests were decreased with increase of FeNPs and FeSO₄ at above 175 mg/L. These findings confirm that the favourable pH values for fermentative hydrogen production were between 6.0 and 6.5. The lowest and highest pH values in the present study were not suitable for fermentative hydrogen production. The similar results have been reported by previous literature those cited in Table 3.

The hydrogen yield and hydrogen content obtained in this study and results from literature are summarized in Table 3. The data showed that the hydrogen yield in this study was higher (2.33 ± 0.09 mol H₂/mol glucose) than those reported in other studies using glucose as substrate. The optimum concentration of Fe²⁺ supplementation was found at 50 mg/L for the production of hydrogen and similar optimum concentration has been reported by Karadag and Puhakka [16]. The Fe²⁺-supplemented experiments showed that the hydrogen yield was comparatively higher than the other reported data. As shown in the Table 3, the results clearly proved that the hydrogen yield was enhanced by the addition of iron oxide nanoparticles when compared to supplementation of Fe²⁺ in both pure and mixed cultures.

Kinetic Analysis of FeNPs Supplementation on Fermentative Hydrogen Production

Shown in Fig. 5 is the effect of different iron oxide nanoparticles concentrations on hydrogen production using *C. acetobutylicum* NCIM 2337 for 24 h. The hydrogen production in control experiment was 254 ± 12 mL, whereas the maximum hydrogen production at 175 mg/L of FeNPs supplementation was 314 ± 4 mL. The results showed that the hydrogen production was improved by the supplementation of FeNPs when compared to control. The obtained hydrogen production data was used to fit the modified Gompertz equation and the kinetic parameters are given in Table 1. The lag phase time was gradually decreased from 8.9 to 6.9 h when the addition of FeNPs was varied from 50 to 175 mg/L. Furthermore, the lag phase time was increased with increase of FeNPs at above 175 mg/L. The lowest lag phase time of 6.9 h was found at 175 mg/L of FeNPs. A similar observation was described earlier [26], the lag-phase time was decreased from 35.4 to 24.4 h when the addition of hematite nanoparticles varied from 25 to 1,600 mg/L for the hydrogen production from sucrose using mixed cultures. From

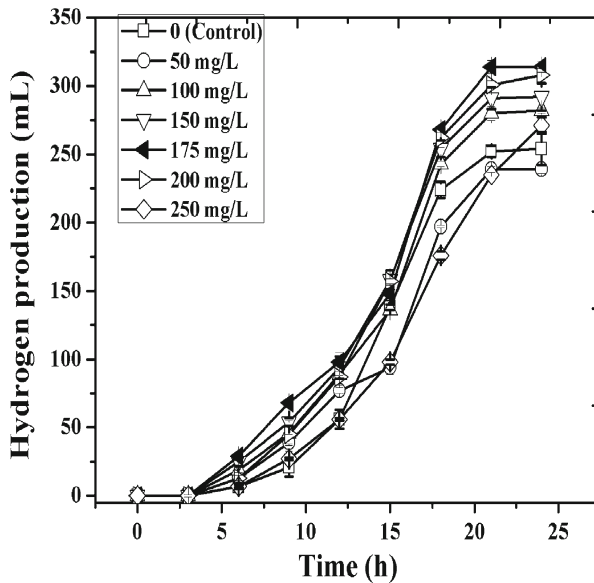


Fig. 5 Hydrogen production versus corresponding fermentation time at different concentrations of iron oxide nanoparticles

Table 1, the maximum hydrogen production rate of 25.3 mL/h was obtained at 175 mg/L of FeNPs.

In addition, the similar hydrogen production rate was found to be at 200 mg/L and it was decreased at the concentration of 250 mg/L of FeNPs. The hydrogen production rate was significantly enhanced by the supplementation of FeNPs with increasing concentration from 50 to 175 mg/L and further it was not favourable to improve the H_2 production rate at concentration over 175 mg/L. This may be due to the fact that the high concentration of FeNPs could inhibit the activity of *C. acetobutylicum*. As noted previously [26], the high initial concentration of hematite nanoparticles promoted the start-up of hydrogen production rate, but the excess soluble hematite nanoparticles was harmful to the microorganisms, and resulted in the decrease of hydrogen production rate. In comparison, the low hydrogen production rate and high lag phase time was observed at all the concentrations of $FeSO_4$ addition (data not shown).

Table 1 Kinetic parameters for hydrogen production at various concentrations of iron oxide nanoparticles

FeNPs Concentration (mg/L)	P (mL)	R_m (mL/h)	λ (h)	R^2
0	254	23	9.2	0.9933
50	239	22.16	8.9	0.9913
100	282	24	8.6	0.9892
150	292	23.3	8.1	0.9848
175	314	25.33	6.9	0.981
200	308	25.3	7.9	0.9913
250	271	19.88	9.65	0.9943

Effect of FeNPs on Soluble Metabolites Distribution

The effects of FeSO₄ and FeNPs on VFA with ethanol concentration are given in Table 2. The formation of VFA and ethanol was affected by the addition of FeSO₄ and FeNPs in batch experiments. The major soluble metabolites produced by *C. acetobutylicum* were acetate, butyrate, propionate and ethanol. The experimental results showed that the soluble metabolites were slightly improved by the addition of FeSO₄ concentration at 50 mg/L, when compared to control. Furthermore, the soluble metabolites were remarkably decreased with increase of FeSO₄ concentration at above 50 mg/L. However, the butyrate concentration was considerably obtained at all concentrations of FeSO₄ when compared to other metabolites. This result indicates that the fermentation process by *C. acetobutylicum* was considered as butyrate fermentation type in control and FeSO₄-supplemented experiments. On the other hand, the concentration of acetate and butyrate yields in batch tests was slightly increased with increase of FeNPs concentrations from 0 to 175 mg/L. The acetate concentration was decreased with increase of FeNPs concentrations at above 175 mg/L, whereas the butyrate concentration was steadily increased with increase of FeNPs as the same. Meanwhile, ethanol and propionate were also increased at above 175 mg/L of FeNPs supplementation. These results exhibit that the high hydrogen content was evident with acetate and butyrate. Further, the ethanol and propionate decreased the hydrogen content. Similar findings were published by Hawkes et al. [27], who reported that the high hydrogen content associated with acetate and butyrate, while other metabolites decreased the hydrogen production. According to theoretical yield, 4 moles of hydrogen is produced from 1 mole of glucose at the acetate fermentation type and 2 moles for butyrate fermentation type as follows (Eqs. 3 and 4).

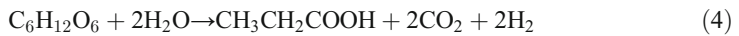
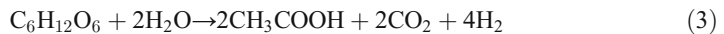


Table 2 Effects of FeSO₄ and FeNPs on soluble metabolites distribution

Exp	Concentration	Ethanol	Acetic acid (mg/L)	Butyric acid	Propionic acid
Control	0	324.3±11.3	789.34±31.2	897.5±6.43	146.4±13.45
FeSO ₄	50	354.4±16.3	814.7±28.3	907.3±24.32	168.3±16.42
	100	298.4±19.3	724.16±33.2	928.4±28.34	138.3±13.23
	150	318.4±14.4	638.29±30.5	878.5±21.24	148.3±28.24
	175	247.3±19.2	539.59±31.2	906.4±23.24	129.4±11.43
	200	214.3±21.2	529.12±29.4	789.4±28.23	132.2±10.24
	250	113.3±22.3	512.4±24.3	657.3±21.1	128.34±12.24
	FeNPs	50	306.2±14.53	792.71±24.3	907.2±33.45
100		265.3±21.23	828.34±26.5	928.4±21.24	114.2±21.34
150		317.3±13.45	839.62±24.3	919.3±22.24	102.5±17.44
175		319.2±16.2	845.82±31.4	924.4±11.4	117.9±19.34
200		331.4±18.3	817.29±20.3	913.5±19.34	124.2±18.34
250		349.1±21.2	719.48±13.2	929.3±17.35	141.2±13.35

Table 3 Comparison of literature data on hydrogen yield and hydrogen content using glucose as a substrate

Microorganism	Operation mode	pH	Substrate concentration (g/L)	Iron concentration (mg/L)	HC ^a (%)	H ₂ yield (mol H ₂ /mol glucose)	Reference
<i>C. acetobutylicum</i>	Continuous	6.0	2.5	–	50	~2.0	[28]
<i>C. acetobutylicum</i> ATCC 824	Continuous	6.2	8.3	–	74	0.9	[29]
<i>C. acetobutylicum</i> ATCC 824	Batch	6.2	7.0	–	25.4	1.79	[30]
<i>C. butyricum</i>	Batch	7.6	5.0	10 ^{-6b}	–	1.08	[25]
Mixed culture	Batch	6.5	9.0	40	42.1	1.59	[31]
Mixed culture	Continuous	5.0	9.0	50	44.7	1.13	[16]
<i>C. acetobutylicum</i> NCIM 2337	Batch	6.0	7.5	–	34	1.74	Present study
				50	40	2.06	
				175 ^c	52	2.33	

^a Hydrogen content^b 10⁻⁶ mol L⁻¹ of Fe/SiO₂ nanoparticles^c Iron oxide nanoparticles

The present study demonstrates that the fermentation process by *C. acetobutylicum* was considered as butyrate fermentation type in control and FeSO₄-supplemented experiments, as represented in Eq. 4. In FeNPs-supplemented experiments, the fermentation type was shifted from butyrate to acetate/butyrate fermentation type as illustrated in Eqs. 3 and 4. This fermentation type was favourable for hydrogen production and produced maximum hydrogen yield of 2.33±0.09 mol H₂/mol glucose, but the considerable co-production of ethanol was found to be a barrier to achieve the theoretical yield (Table 3). The supplementation of FeNPs played a crucial role in fermentative pathway to form an acetate/butyrate fermentation type. Moreover, this metabolic pathway shifted to solventogenesis phase at above 175 mg/L. Nevertheless, it is important to maintain the fermentation at acidogenesis condition to produce efficient hydrogen production from *C. acetobutylicum*.

Conclusions

In this work, iron oxide nanoparticles were successfully synthesized using *M. koenigii* leaf extract and their effect of enhancement on fermentative hydrogen production by *C. acetobutylicum* NCIM 2337 was investigated. *M. koenigii* is an evergreen plant and its leaves are easily available in all four seasons. Thus, it can be used for the rapid green synthesis of iron oxide nanoparticles instead of chemical synthesis and other biosynthesis. The strong absorption band of 580 cm⁻¹ in FTIR spectra indicated the formation of maghemite (γ-Fe₂O₃). The appearance of strong vibrational bands including amide 1, –C–N and –OH groups in biomolecules showed the presence of flavonoids, alkaloids and polyphenols in curry leaf. Hence, these biomolecules seem to be responsible for reduction and stabilization of iron oxide nanoparticles. The present study demonstrates that the maximum hydrogen production of 314 ±4 mL, hydrogen content of 52±0.8 % and hydrogen yield of 2.33±0.09 mol H₂/mol glucose were achieved by the addition of optimum concentration of 175 mg/L iron oxide nanoparticles.

The enhancement of hydrogenase activity by the supplementation of iron oxide nanoparticles was believed to be accountable for high yield of hydrogen production.

Acknowledgments This research was funded by the Department of Biotechnology (Ref. No. BT/PR12051/PBD/26/213/2009, dated 19 November 2010), New Delhi, India. The author Mohanraj gratefully thank the Ministry of New and Renewable Energy, New Delhi, India, for the Senior Research Fellowship (NREF–SRF).

References

1. Teja, A. S., & Koh, P. Y. (2009). Synthesis, properties, and applications of magnetic iron oxide Nanoparticles. *Progress in Crystal Growth and Characterization of Materials*, 55, 22–45.
2. Matei, E., Predescu, A., Vasile, E., & Predescu, A. (2011). Properties of magnetic iron oxides used as materials for wastewater treatment. *Journal of Physics: Conference Series*, 304, 012022.
3. Safarikova, M., Maderova, Z., & Safarik, I. (2009). Ferrofluid modified *Saccharomyces cerevisiae* cells for biocatalysis. *Food Research International*, 42, 521–524.
4. Narayanan, K. B., & Sakthivel, N. (2010). Biological synthesis of metal nanoparticles by Microbes. *Advance in Colloid and Interface Science*, 156, 1–13.
5. Shahwan, T., Sirriah, S. A., Nairat, M., Boyaci, E., Eroglu, A. E., Scott, T. B., & Hallam, K. R. (2011). Green synthesis of iron nanoparticles and their application as a Fenton-like catalyst for the degradation of aqueous cationic and anionic dyes. *Chemical Engineering Journal*, 172, 258–266.
6. Hoag, G. E., Collins, J. B., Holcomb, J. L., Hoag, J. R., Nadagouda, M. N., & Varma, R. S. J. (2009). Degradation of bromothymol blue by greener nano scale zero valent iron synthesized using tea polyphenols. *Journal of Material Chemistry*, 19, 8671–8677.
7. Nadagouda, M. N., Castle, A. B., Murdock, R. C., Hussain, S. M., & Varma, R. S. (2010). In vitro biocompatibility of nanoscale zerovalent iron particles (NZVI) synthesised using tea polyphenols. *Green Chemistry*, 12, 114–122.
8. Cai, Y., Shen, Y., Xie, A., Li, S., & Wang, X. (2010). Green synthesis of soya bean sprouts-mediated superamagnetic Fe₃O₄ nanoparticles. *Journal of Magnetism and Magnetic Materials*, 322, 2938–2943.
9. Njagi, E. C., Huang, H., Stafford, L., Genuino, H., Galindo, H. M., Collins, J. B., Hoag, G. E., & Suib, S. L. (2011). Biosynthesis of iron and silver nanoparticles at room temperature using aqueous sorghum bran extracts. *Langmuir*, 27, 264–271.
10. Philip, D., Unni, C., Aromal, S. A., & Vidhu, V. K. (2011). *Murraya koenigii* leaf assisted rapid green synthesis of silver and gold nanoparticles. *Spectrochimica Acta Part A: Molecular and Biomolecular Spectroscopy*, 78, 899–904.
11. Christensen, L., Vivekanandhan, S., Misra, M., & Mohanty, A. K. (2011). Biosynthesis of silver nanoparticles using *Murraya koenigii* (curry leaf): an investigation on the effect of broth concentration in reduction mechanism and particle size. *Advances Material Letters*, 2, 429–434.
12. Wang, A., Ren, N., Shi, Y., & Lee, D. J. (2008). Bioaugmented hydrogen production from microcrystalline cellulose using co-culture - *Clostridium acetobutylicum* X9 and *Ethanoigenens harbinense* B49. *International Journal of Hydrogen Energy*, 33, 912–917.
13. Chong, M. L., Sabaratnam, V., Shirai, Y., & Hassan, M. A. (2009). Biohydrogen production from biomass and industrial waste by dark fermentation. *International Journal of Hydrogen Energy*, 34, 3277–3287.
14. Liu, B. F., Ren, N. Q., Ding, J., Xie, G. J., & Guo, W. Q. (2009). The effect of Ni²⁺, Fe²⁺ and Mg²⁺ concentration on photo-hydrogen production by *Rhodospseudomonas faecalis* RLD-53. *International Journal of Hydrogen Energy*, 34, 721–726.
15. Wang, J., & Wan, W. (2008). Effect of Fe²⁺ concentration on Fermentative hydrogen production by mixed cultures. *International Journal of Hydrogen Energy*, 33, 1215–1220.
16. Karadag, D., & Puhakka, J. A. (2010). Enhancement of anaerobic hydrogen production by iron and nickel. *International Journal of Hydrogen Energy*, 35, 8554–8560.
17. Dubois, M., Gilles, K. A., Hamilton, J. K., Rebers, P. A., & Smith, F. (1956). Colorimetric method for determination of sugars and related substances. *Analytical Chemistry*, 28, 350–356.
18. Cappelletti, B. M., Reginatto, V., Amante, E. R., & Antonio, R. V. (2011). Fermentative production of hydrogen from cassava processing wastewater by *Clostridium acetobutylicum*. *Renewable Energy*, 36, 3367–3372.
19. Mie, G. (1908). Beitrage zur Optik truber medien speziell kolloidaler metallosungen. *Annals of Physics*, 330, 377–445.

20. Guo, L., Huang, Q., Li, X., & Yang, S. (2001). Iron nanoparticles: synthesis and applications in surface enhanced raman scattering and electrocatalysis. *Physical Chemistry Chemical Physics*, *3*, 1661–1665.
21. Narayanan, K. B., & Sakthivel, N. (2011). Extracellular synthesis of silver nanoparticles using the leaf extract of *coleus amboinicus* Lour. *Materials Research Bulletin*, *46*, 1708–1713.
22. Togashi, T., Naka, T., Asahina, S., Sato, K., Takami, S., & Adschiri, T. (2011). Surfactant-assisted one-pot synthesis of supermagnetic magnetite nanoparticle clusters tunable cluster size and magnetic field sensitivity. *Dalton Transactions*, *40*, 1073–1078.
23. Biswas, S., Belfield, K. D., Das, R. K., Ghosh, S., & Hebard, A. F. (2012). Supermagnetic nanocomposites template with pyrazole-containing diblock copolymers. *Polymers*, *4*, 1211–1225.
24. Babu, S. A., & Prabu, H. G. (2011). Synthesis of AgNPs using the extract of *Calotropis procera* flower at room temperature. *Material Letters*, *65*, 1675–1677.
25. Beckers, L., Hilgsmann, S., Lambert, S. D., Heinrichs, B., & Thonart, P. (2013). Improving effect of metal and oxide nanoparticles encapsulated in porous silica on fermentative biohydrogen production by *Clostridium butyricum*. *Bioresource Technology*, *133*, 109–117.
26. Han, H., Cui, M., Wei, L., Yang, H., & Shen, J. (2011). Enhancement effect of hematite nanoparticles on fermentative hydrogen production. *Bioresource Technology*, *102*, 7903–7909.
27. Hawkes, F. R., Dinsdale, R., Hawkes, D. L., & Hussy, I. (2002). Sustainable fermentative hydrogen production: challenges for process optimisation. *International Journal of Hydrogen Energy*, *27*, 1339–1347.
28. Chin, H. L., Chen, Z. S., & Chou, C. P. (2003). Fedbatch operation using *Clostridium acetobutylicum* suspension culture as biocatalyst for enhancing hydrogen production. *Biotechnology Progress*, *19*, 383–388.
29. Zhang, H., Bruns, M. A., & Logan, B. E. (2006). Biological hydrogen production by *Clostridium acetobutylicum* in an unsaturated flow reactor. *Water Research*, *40*, 728–734.
30. Oh, S. E., Zuo, Y., Zhang, H., Guiltinan, M. J., Logan, B. E., & Regan, J. M. (2009). Hydrogen production by *Clostridium acetobutylicum* ATCC 824 and megaplasmid-deficient mutant M5 evaluated using a large headspace volume technique. *International Journal of Hydrogen Energy*, *34*, 9347–9353.
31. Karadag, D., Makinen, A. E., Efimova, E., & Puhakka, J. A. (2009). Thermophilic biohydrogen production by an anaerobic heat treated-hot spring culture. *Bioresource Technology*, *100*, 5790–5795.